

Signal recognition and adapted filtering by non-commutative tomography

Carlos Aguirre *

GNB, Escuela Politécnica Superior,
Universidad Autónoma de Madrid, Campus de Cantoblanco,
Ctra de Colmenar Km 16, 28049 Madrid, Spain

R. Vilela Mendes †

CMAF, Complexo Interdisciplinar,
Av. Gama Pinto 2, 1649-003 Lisboa, Portugal
IPFN, Instituto Superior Técnico,
Av. Rovisco Pais 1, 1049-001 Lisboa

Abstract

Tomograms, a generalization of the Radon transform to arbitrary pairs of non-commuting operators, are positive bilinear transforms with a rigorous probabilistic interpretation which provide a full characterization of the signal and are robust in the presence of noise. Tomograms based on the time-frequency operator pair, were used in the past for component separation and denoising. Here we show how, by the construction of an operator pair adapted to the signal, meaningful information with good time resolution is extracted even in very noisy situations.

Keywords: Integral transforms, Tomograms, Filtering

*e-mail: carlos.aguirre@uam.es

†e-mail: rvilela.mendes@gmail.com

1 Introduction

1.1 Integral transforms: linear, bilinear and tomograms

Integral transforms [1] [2] are very useful for signal processing in communications, engineering, medicine, physics, etc. Linear and bilinear transforms have been used. Among the linear transforms, Fourier [3] and wavelets [4] [5] [6] are the most popular. Among the bilinear ones, the Wigner–Ville quasidistribution [7] [8] is the most commonly used to provide information in the joint time–frequency domain. A joint time–frequency description of signals is indeed important, because in many applications (biomedical, seismic, radar, etc.) the signals are of finite (sometimes very short) duration. However, the oscillating cross-terms in the Wigner–Ville and other quasidistributions [9] [10] [11] make the interpretation of these transforms a difficult matter. Even when the average of the cross-terms is small, their amplitude may be greater than the signal in time–frequency regions that carry no physical information.

The difficulties with the physical interpretation of quasidistributions arise from the fact that time and frequency correspond to two noncommutative operators. Hence a joint probability density can never be defined. Even in the case of positive quasiprobabilities like the Husimi–Kano function [12] [13], an interpretation as a joint probability distribution is also not possible because the two arguments of the function are not simultaneously measurable random variables.

Recently, a new type of strictly positive bilinear transform has been proposed [14] [15] [16], called *tomogram*, which is a generalization of the Radon transform [17] to arbitrary noncommutative pairs of operators. The Radon–Wigner transform [18] [19] is a particular case of such noncommutative tomography technique. The tomograms are strictly positive probability densities, provide a full characterization of the signal and are robust in the presence of noise.

A unified framework to characterize linear transforms, quasidistributions and tomograms was developed in Ref.[15]. To fix notation we briefly review it here. Signals $f(t)$ are considered as vectors $|f\rangle$ in a subspace \mathcal{N} of a Hilbert space \mathcal{H} with dual space \mathcal{N}^* . Then a family of unitary operators $U(\alpha) = e^{iB(\alpha)}$, α being a label $\{\alpha \in I, I \subset \mathbb{R}^n\}$, is defined on \mathcal{N}^* . Using a ket-bra notation we denote $|f\rangle \in \mathcal{N}$ and $\langle f| \in \mathcal{N}^*$. In this setting three types of integral transforms are constructed. Let $h \in \mathcal{N}^*$ be a reference vector and let U be such that the linear span of $\{U(\alpha)h \in \mathcal{N}^* : \alpha \in I\}$ is dense in \mathcal{N}^* .

In $\{U(\alpha)h\}$, a complete set of vectors can be chosen to serve as basis.

1 - Linear transforms

$$W_f^{(h)}(\alpha) = \langle U(\alpha)h | f \rangle \quad (1)$$

2 - Quasi-distributions

$$Q_f(\alpha) = \langle U(\alpha)f | f \rangle \quad (2)$$

3 - Tomograms

Given an unitary $U(\alpha) = e^{iB(\alpha)}$, $B(\alpha)$ has the spectral projection $B(\alpha) = \int XP(X) dX$. Let

$$P(X) \doteq |X\rangle \langle X|$$

be the projector¹ on the (generalized) eigenvector $\langle X| \in \mathcal{N}^*$ of $B(\alpha)$. The tomogram is

$$M_f^{(B)}(X) = \langle f | P(X) | f \rangle = \langle f | X \rangle \langle X | f \rangle = |\langle X | f \rangle|^2 \quad (3)$$

The tomogram $M_f^{(B)}(X)$ is the squared amplitude of the projection of the signal $|f\rangle \in \mathcal{N}$ on the eigenvector $\langle X| \in \mathcal{N}^*$ of the operator $B(\alpha)$. Therefore it is positive. For normalized $|f\rangle$,

$$\langle f | f \rangle = 1$$

the tomogram is normalized

$$\int M_f^{(B)}(X) dX = 1 \quad (4)$$

and may be interpreted as a probability distribution on the set of generalized eigenvalues of $B(\alpha)$, that is, as the probability distribution for the random variable X corresponding to the observable defined by the operator $B(\alpha)$.

The tomogram is a homogeneous function

$$M_f^{(B/p)}(X) = |p| M_f^{(B)}(pX) \quad (5)$$

¹Another convenient notation for the projector on a generalized eigenvector of $B(\alpha)$ with eigenvalue X is

$$\delta(B(\alpha) - X) \doteq P(X)$$

Examples:

If $U(\alpha)$ is unitary generated by $B_F(\vec{\alpha}) = \alpha_1 t + i\alpha_2 \frac{d}{dt}$ and h is a (generalized) eigenvector of the time-translation operator the linear transform $W_f^{(h)}(\alpha)$ is the Fourier transform. For the same $B_F(\vec{\alpha})$, the quasi-distribution $Q_f(\alpha)$ is the ambiguity function and the Wigner–Ville transform [7] [8] is the quasi-distribution $Q_f(\alpha)$ for the following B -operator

$$B^{(WV)}(\alpha_1, \alpha_2) = -i2\alpha_1 \frac{d}{dt} - 2\alpha_2 t + \frac{\pi \left(t^2 - \frac{d^2}{dt^2} - 1 \right)}{2} \quad (6)$$

The wavelet transform is $W_f^{(h)}(\alpha)$ for $B_W(\vec{\alpha}) = \alpha_1 D + i\alpha_2 \frac{d}{dt}$, D being the dilation operator $D = -\frac{1}{2} \left(it \frac{d}{dt} + i \frac{d}{dt} t \right)$. The wavelets $h_{s,\tau}(t)$ are kernel functions generated from a basic wavelet $h(\tau)$ by means of a translation and a rescaling ($-\infty < \tau < \infty$, $s > 0$):

$$h_{s,\tau}(t) = \frac{1}{\sqrt{s}} h\left(\frac{t-\tau}{s}\right) \quad (7)$$

using the operator

$$U^{(A)}(\tau, s) = \exp(i\tau\hat{\omega}) \exp(i \log s D), \quad (8)$$

$$h_{s,\tau}(t) = U^{(A)\dagger}(\tau, s)h(t). \quad (9)$$

The Bertrand transform [20] [21] is the quasi-distribution $Q_f(\alpha)$ for B_W . Linear, bilinear and tomogram transforms are related to one another (see [15]).

1.2 Tomograms: Some examples

As shown above, tomograms are obtained from projections on the eigenstates of the B operators. These operators may be linear combinations of different (commuting or noncommuting) operators,

$$B = \mu O_1 + \nu O_2$$

meaning that the tomogram explores the signal along lines in the plane (O_1, O_2) . For example for

$$B(\mu, \nu) = \mu t + \nu \omega = \mu t + i\nu \frac{d}{dt}$$

the tomogram is the expectation value of a projection operator with support on a line in the time–frequency plane

$$X = \mu t + \nu \omega \quad (10)$$

Therefore, $M_f^{(S)}(X, \mu, \nu)$ is the marginal distribution of the variable X along this line in the time–frequency plane. The line is rotated and rescaled when one changes the parameters μ and ν . In this way, the whole time–frequency plane is sampled and the tomographic transform contains all the information on the signal. Instead of marginals collected along straight lines on the time–frequency plane, one may use other curves to sample this space [15].

Tomograms associated to the generators of the conformal group:

Time-frequency

$$B_1 = \mu t + i\nu \frac{d}{dt} \quad (11)$$

Time-scale

$$B_2 = \mu t + i\nu \left(t \frac{d}{dt} + \frac{1}{2} \right) \quad (12)$$

Frequency-scale

$$B_3 = i\mu \frac{d}{dt} + i\nu \left(t \frac{d}{dt} + \frac{1}{2} \right) \quad (13)$$

Time-conformal

$$B_4 = \mu t + i\nu \left(t^2 \frac{d}{dt} + t \right) \quad (14)$$

The construction of the tomograms reduces to the calculation of the generalized eigenvectors of each one of the B_i operators

$$B_1 \psi_1(\mu, \nu, t, X) = X \psi_1(\mu, \nu, t, X)$$

$$\psi_1(\mu, \nu, t, X) = \exp i \left(\frac{\mu t^2}{2\nu} - \frac{tX}{\nu} \right) \quad (15)$$

with normalization

$$\int dt \psi_1^*(\mu, \nu, t, X) \psi_1(\mu, \nu, t, X') = 2\pi\nu \delta(X - X') \quad (16)$$

$$B_2 \psi_2(\mu, \nu, t, X) = X \psi_2(\mu, \nu, t, X)$$

$$\psi_2(\mu, \nu, t, X) = \frac{1}{\sqrt{|t|}} \exp i \left(\frac{\mu t}{\nu} - \frac{X}{\nu} \log |t| \right) \quad (17)$$

$$\int dt \psi_2^*(\mu, \nu, t, X) \psi_2(\mu, \nu, t, X') = 4\pi\nu\delta(X - X') \quad (18)$$

$$B_3\psi_3(\mu, \nu, \omega, X) = X\psi_3(\mu, \nu, \omega, X)$$

$$\psi_3(\mu, \nu, t, X) = \exp(-i) \left(\frac{\mu}{\nu}\omega - \frac{X}{\nu} \log|\omega| \right) \quad (19)$$

$$\int d\omega \psi_1^*(\mu, \nu, \omega, X) \psi_1(\mu, \nu, \omega, X') = 2\pi\nu\delta(X - X') \quad (20)$$

$$B_4\psi_4(\mu, \nu, t, X) = X\psi_4(\mu, \nu, t, X)$$

$$\psi_4(\mu, \nu, t, X) = \frac{1}{|t|} \exp i \left(\frac{X}{\nu t} + \frac{\mu}{\nu} \log|t| \right) \quad (21)$$

$$\int dt \psi_4^*(\mu, \nu, t, s) \psi_4(\mu, \nu, t, s') = 2\pi\nu\delta(s - s') \quad (22)$$

Then the tomograms are:

Time-frequency tomogram

$$M_1(\mu, \nu, X) = \frac{1}{2\pi|\nu|} \left| \int \exp \left[\frac{i\mu t^2}{2\nu} - \frac{itX}{\nu} \right] f(t) dt \right|^2 \quad (23)$$

Time-scale tomogram

$$M_2(\mu, \nu, X) = \frac{1}{2\pi|\nu|} \left| \int dt \frac{f(t)}{\sqrt{|t|}} e^{[i(\frac{\mu}{\nu}t - \frac{X}{\nu} \log|t|)]} \right|^2 \quad (24)$$

Frequency-scale tomogram

$$M_3(\mu, \nu, X) = \frac{1}{2\pi|\nu|} \left| \int d\omega \frac{f(\omega)}{\sqrt{|\omega|}} e^{[-i(\frac{\mu}{\nu}\omega - \frac{X}{\nu} \log|\omega|)]} \right|^2 \quad (25)$$

$f(\omega)$ being the Fourier transform of $f(t)$

Time-conformal tomogram

$$M_4(\mu, \nu, X) = \frac{1}{2\pi|\nu|} \left| \int dt \frac{f(t)}{|t|} e^{[i(\frac{X}{\nu t} + \frac{\mu}{\nu} \log|t|)]} \right|^2 \quad (26)$$

The tomograms M_1 , M_2 and M_4 interpolate between the (squared) time signal ($\nu = 0$) and its projection on the $\psi_i(\mu, \nu, t, X)$ functions for $\mu = 0$.

In a similar way, tomograms may be constructed for any operator of the general type

$$B_4 = \mu t + i\nu \left(g(t) \frac{d}{dt} + \frac{1}{2} \frac{dg(t)}{dt} \right)$$

the generalized eigenvectors being

$$\psi_g(\mu, \nu, t, X) = |g(t)|^{-1/2} \exp i \left(-\frac{X}{\nu} \int^t \frac{ds}{g(s)} + \frac{\mu}{\nu} \int^t \frac{s ds}{g(s)} \right)$$

When dealing with finite-time signals and finite-time tomograms some normalization modifications are needed. For example, for a time-frequency tomogram, instead of (23), we consider the finite-time tomogram, for a signal defined from t_0 to $t_0 + T$

$$M_1(\theta, X) = \left| \int_{t_0}^{t_0+T} f^*(t) \psi_{\theta, X}^{(1)}(t) dt \right|^2 = |\langle f, \psi^{(1)} \rangle|^2 \quad (27)$$

with

$$\psi_{\theta, X}^{(1)}(t) = \frac{1}{\sqrt{T}} \exp \left(\frac{i \cos \theta}{2 \sin \theta} t^2 - \frac{iX}{\sin \theta} t \right) \quad (28)$$

and $\mu = \cos \theta$, $\nu = \sin \theta$. θ is a parameter that interpolates between the time and the frequency operators, running from 0 to $\pi/2$ whereas X is allowed to be any real number. An orthonormalized set of $\psi_{\theta, X}^{(1)}(t)$ vectors is obtained by choosing the sequence

$$X_n = X_0 + \frac{2n\pi}{T} \sin \theta \quad n \in \mathbb{Z} \quad (29)$$

Likewise for the finite-time time-scale tomogram $M_2(\mu, \nu, X)$ (Eq.24) and the finite-time time-conformal tomogram $M_4(\mu, \nu, X)$ (Eq.26):

$$M_2(\theta, X) = \left| \int_{t_0}^{t_0+T} f^*(t) \psi_{\theta, X}^{(2)}(t) dt \right|^2 = |\langle f, \psi^{(2)} \rangle|^2 \quad (30)$$

$$\psi_{\theta, X}^{(2)}(t) = \frac{1}{\sqrt{\log |t_0 + T| - \log |t_0|}} \frac{1}{\sqrt{|t|}} \exp i \left(\frac{\cos \theta}{\sin \theta} t - \frac{X}{\sin \theta} \log |t| \right) \quad (31)$$

$$X_n = X_0 + \frac{2n\pi}{\log |t_0 + T| - \log |t_0|} \sin \theta \quad n \in \mathbb{Z} \quad (32)$$

and

$$M_4(\theta, X) = \left| \int_{t_0}^{t_0+T} f^*(t) \psi_{\theta, X}^{(4)}(t) dt \right|^2 = |\langle f, \psi^{(4)} \rangle|^2 \quad (33)$$

$$\psi_{\theta, X}^{(4)}(t) = \sqrt{\frac{t_0(t_0+T)}{T}} \frac{1}{|t|} \exp i \left(\frac{\cos \theta}{\sin \theta} \log |t| + \frac{X}{t \sin \theta} \right) \quad (34)$$

$$X_n = X_0 + \frac{t_0(t_0+T)}{T} 2\pi n \sin \theta \quad n \in \mathbb{Z} \quad (35)$$

2 Applications of tomograms: Denoising, and component separation

Most natural and man-made signals are nonstationary and have a multicomponent structure. Therefore separation of its components is an issue of great technological relevance. However, the concept of signal component is not uniquely defined. The notion of *component* depends as much on the observer as on the observed object. When we speak about a component of a signal we are in fact referring to a particular feature of the signal that we want to emphasize. For signals that have distinct features both in time and in the frequency domain, the time-frequency tomogram is an appropriate tool.

Consider finite-time tomograms as in (27). For all different θ 's the $U(\theta)$, of which $B(\theta)$ is the self-adjoint generator, are unitarily equivalent operators, hence all the tomograms share the same information.

First we would select a subset X_n in such a way that the corresponding family $\{\psi_{\theta, X_n}^{(1)}(t)\}$ is orthogonal and normalized,

$$\langle \psi_{\theta, X_n}^{(1)} \psi_{\theta, X_m}^{(1)} \rangle = \delta_{m,n} \quad (36)$$

This is the sequence listed in (29), where X_0 is freely chosen (in general we take $X_0 = 0$). We then consider the projections of the signal $f(t)$ on this set of $\psi_{\theta, X_n}^{(1)}$ vectors

$$c_{X_n}^\theta(f) = \langle f, \psi_{\theta, X_n}^{(1)} \rangle \quad (37)$$

Denoising consists in eliminating the $c_{X_n}^\theta(f)$ such that

$$|c_{X_n}^\theta(f)|^2 \leq \epsilon \quad (38)$$

for some threshold ϵ . This power selective denoising is more robust than, for example, frequency filtering which may also eliminate important signal information.

The *component separation technique* is based on the search for an intermediate value of θ where a good compromise might be found between time localization and frequency information. This is achieved by selecting subsets \mathcal{F}_k of the X_n and reconstructing partial signals (k -components) by restricting the sum to

$$f_k(t) = \sum_{n \in \mathcal{F}_k} c_{X_n}^\theta(f) \psi_{\theta, X_n}(t) \quad (39)$$

for each k .

3 Signal detection with an adapted operator pair

Time-frequency tomograms have been used for denoising and component separation of finite-time signals [14] [22] [23] [24] [25]. Time-frequency tomograms are particularly appropriate to identify the time unfolding of the frequency features of the signals. For example, the component separation success [22] [23] in the plasma reflectometry applications is to a large extent due to the fact that the plasma is sampled by microwave chirps and the basis in (28) is exactly a chirp basis. This suggests that, for other types of signals, other types of tomograms should be chosen.

In particular, if in the linear combination $B(\mu, \nu) = \mu t + \nu O$, one chooses an operator O , that is specially tuned to the features of the signal that one wants to extract, then, by looking for the particular values of the set (μ, ν) where the noise effects might cancel out, we may separate the information of very small signals from large noise and also obtain reliable information on the temporal structure of the signal. This would provide a signal-adapted filtering technique. The construction of the operator suited to particular signals may be done by the same techniques that are used in the bi-orthogonal decomposition [26].

The method for the construction of the adapted operator pair is as follows:

Consider a set of N -dimensional time sequences $\{\vec{x}_1, \dots, \vec{x}_k\}$, typical of the signal one wants to detect. For a communication point of view these may be considered as the code words that, later on, one wishes to detect in

a noisy signal. Form the $k \times N$ matrix $U \in \mathcal{M}_{k \times N}$.

$$U = \begin{pmatrix} x_1(1\Delta t) & x_1(2\Delta t) & \dots & x_1(N\Delta t) \\ \vdots & \vdots & & \vdots \\ x_k(1\Delta t) & x_k(2\Delta t) & \dots & x_k(N\Delta t) \end{pmatrix} \quad (40)$$

with $k < N$ typically.

Now construct the square matrices $A = U^T U \in \mathcal{M}_{N \times N}$ and $B = U U^T \in \mathcal{M}_{k \times k}$. The diagonalization of A provides k non-zero eigenvalues $(\alpha_1, \dots, \alpha_k)$ and its corresponding orthogonal N -dimensional eigenvectors (Φ_1, \dots, Φ_k) , $\Phi_j \in \mathbb{R}^N$. Correspondingly, the diagonalization of B would provide the same k eigenvalues and eigenvectors (Ψ_1, \dots, Ψ_k) with $\Psi_j \in \mathbb{R}^k$. If needed one may obtain, by the Gram-Schmidt method, the remaining $N - k$ eigenvectors to span \mathbb{R}^N , which in this context are associated to the eigenvalue zero.

The linear operator S constructed from the set of typical signals is

$$S = \sum_{i=1}^k \alpha_i \Phi_i \Phi_i^t \quad (41)$$

where $S \in \mathcal{M}_{N \times N}$.

For the tomogram we consider an operator $B(\mu, \nu)$ of the form

$$B(\mu, \nu) = \mu t + \nu S = \mu \begin{pmatrix} 1\Delta t & & & & \\ & 2\Delta t & & & \\ & & 3\Delta t & & \\ & & & \ddots & \\ & & & & N\Delta t \end{pmatrix} + \nu \sum_{i=1}^k \alpha_i \Phi_i \Phi_i^t \quad (42)$$

where $B \in \mathcal{M}_{N \times N}$.

The eigenvectors of each $B(\mu, \nu)$ are the columns of the matrix that diagonalizes it. From the projections of a signal on these eigenvectors one constructs a tomogram adapted to the operator pair (t, S) .

3.1 Examples

Here we present some examples of the application of the technique described in the previous Section.

In the first example a set of 40 random signals with pulses of duration $\Delta t = 10$ and intensities $+1$ or -1 are generated. The total length of the

signal is 200 time units. These random signals form the typical data to which we will adapt the tomogram, by constructing the operator S in (41). Fig.1 shows 10 signals of this type. They all vary between $+1$ and -1 , being shifted in the figure for clarity purposes.

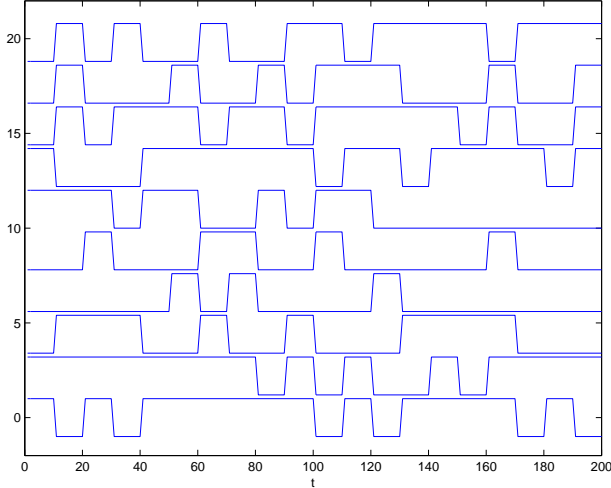


Figure 1: A set of typical signals.

Once the operator S is constructed, one considers the operator

$$B(\theta) = t \cos \theta + S \sin \theta$$

for which one computes the eigenbasis which is used to project the signals to be analyzed. To a pure signal of the same type as those used to construct the operator S (in the upper left panel of Fig.2), we add Gaussian noise (upper right panel of Fig.2). This signal is then analyzed and a tomogram constructed for 20 different values of θ at intervals $\Delta\theta = \pi/40$. A contour plot of the tomogram is shown in the lower left panel of Fig.2. As we have explained before, by inspection of the power distribution in the tomogram one may either select the components of intensity higher than a threshold for denoising of the whole signal or select particular components of signal. In this case what is of interest is to select the part of the signal that corresponds to the typical signals used to construct S . This is done by selecting only the strongest components at the region where they concentrate. In the lower right panel of Fig.2 we show the result of projecting on the eigenvectors 185 to 200 at $\theta_{19} = 19\pi/40$.

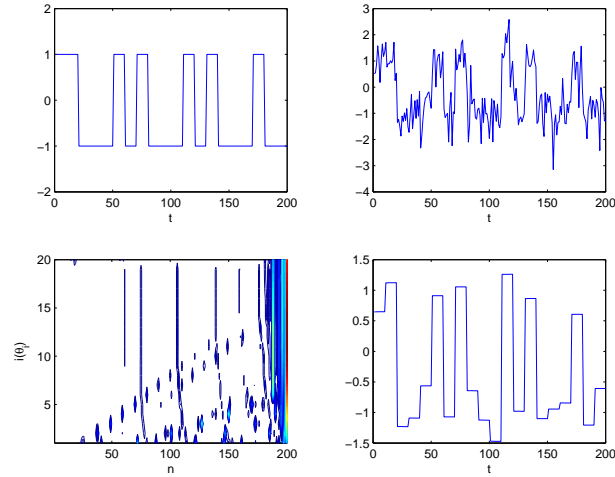


Figure 2: Signal, noisy signal, the tomogram and the projection on the eigenvectors 185 to 200 at $\theta = 19\pi/40$

One sees that the signal is reasonably reconstructed from the noisy input. With a clipping operation at ± 0.5 the reconstruction would be perfect.

For the second example we have generated, as typical signals a set of 40 sines with random frequencies. Fig.3 displays some examples.

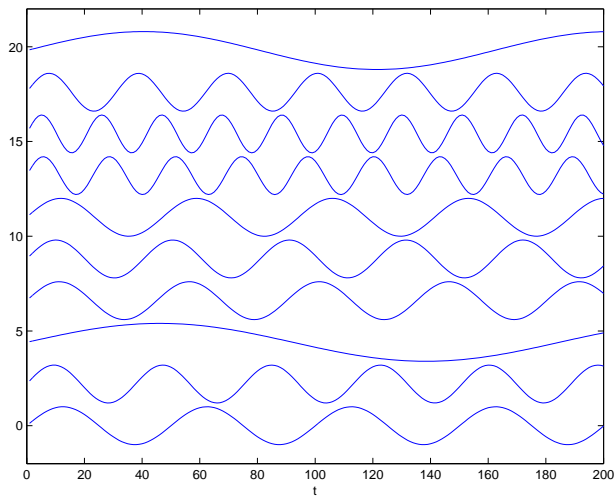


Figure 3: A set of sines with random frequencies

This case is harder because noise (or interference) is expected to contain frequencies similar to the typical signals. Fig.4 shows the results of a typical analysis of a signal that contains pieces of sines at different time intervals. In the upper left panel it is the signal, in the upper right panel the signal with Gaussian noise added, in the lower left panel the tomogram and in the lower right panel the result of the projection on the eigenvectors 189 to 197 at $\theta_4 = 15\pi/40$.

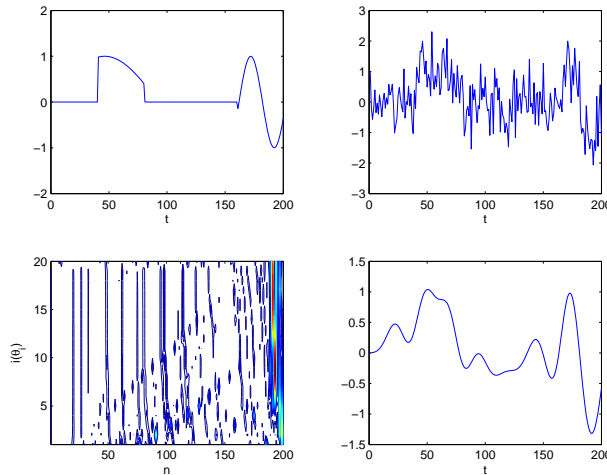


Figure 4: Signal, noisy signal, the tomogram and the projection on the eigenvectors 189 to 197 at $\theta = 19\pi/40$

The projection range that was used aimed at including all the strongest components. Notice however that by selecting particular regions of the tomogram one may extract particular components of the signal. For example, Fig.5 shows the result of projection on the eigenvectors 190 to 199 at $\theta = \pi/10$.

For the third example we use data obtained from the Phoenix Mars Lander [27]. A dust devil is a hot whirlwind generated by a huge contrast between the martian atmospheric air and the planet surface. Dust devils appear in both temperature and pressure data as sudden drops with a duration between two and three minutes. The upper left panel in Figure 6 shows some data from the Phoenix Mars Lander covering a 2000 seconds interval with a sampling rate of $.5Hz$. A dust devil is clearly visible at $t \simeq 800s$ as a drop in the pressure value.

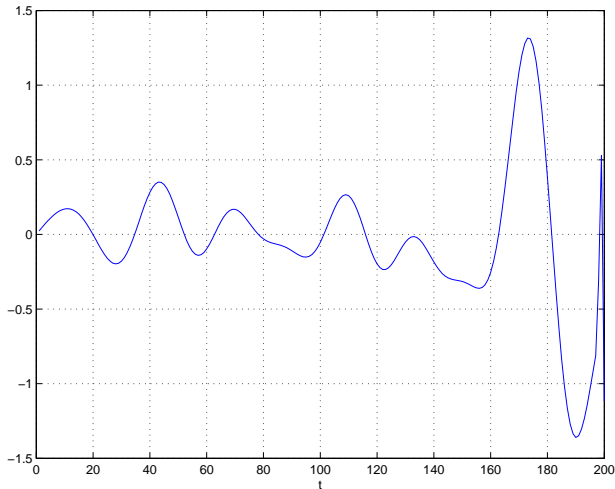


Figure 5: The projection on the eigenvectors 190 to 199 at $\theta = \pi/10$ which separates the second time component of the signal

There has been several efforts to develop systematic methods to detect the effect of dust devils on the martian atmosphere data. They are based either on checking several ad-hoc conditions in the data [27] or on Field-Programmable Gate Arrays (FPGAs) [28].

To use our adapted tomographic filtering method for the detection of dust devils we have generated a set of 278 signals that resemble the shape that a dust devil produces on the data, that is a sudden drop of about 3% from the baseline, with different durations ranging from 60 to 80 time units. The upper right panel displays several of these typical signals. Some of the signals have been shifted up or down for representation purposes.

As in the previous examples a tomogram is constructed for 20 different values of θ at intervals $\Delta\theta = \pi/40$. A contour plot of the first 999 coefficients of the tomogram is shown in the lower left panel of Figure 6. Coefficient $n = 1000$ corresponds to the biggest eigenvalue (and its corresponding eigenvector). This eigenvector contains most of the energy of the signal, and is several orders of magnitude bigger than any other coefficient, so clearly this coefficient has not been plotted in the tomogram. By direct inspection, we observe that, besides the coefficient $n = 1000$, the strongest components concentrate close to $n = 400$. The lower right panel in figure 6 shows the projection on the eigenvectors 340 to 450 and 1000 at $\theta = 19\pi/40$. One sees

that the pressure drop produced by the dust devil is very well reconstructed and separated from any other components present in the signal such as noise or smaller pressure variations.

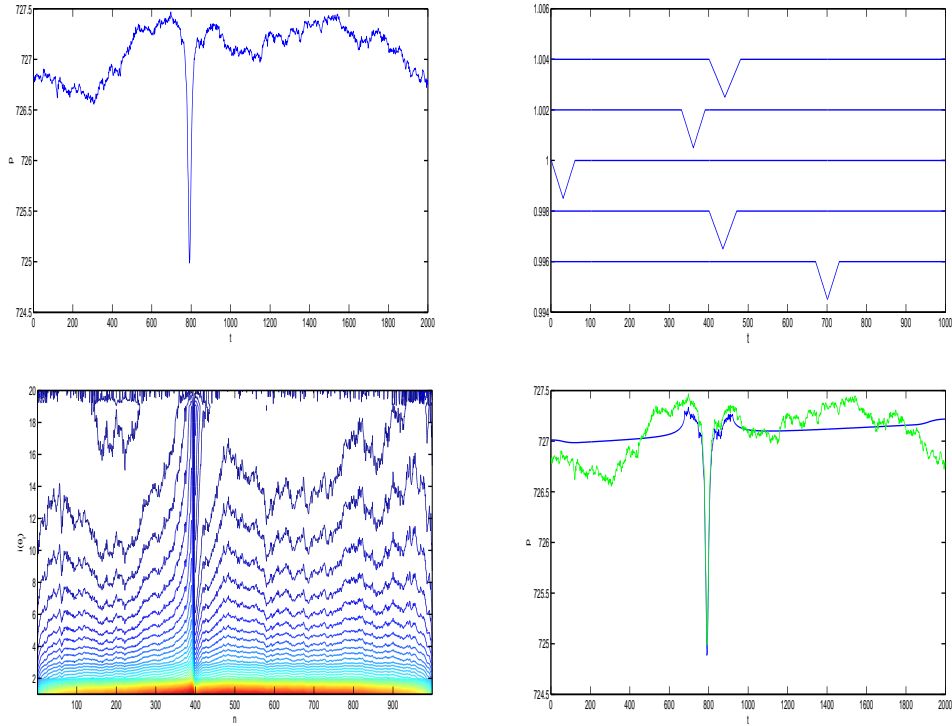


Figure 6: Signal, typical signals, the tomogram (coefs 1-999) and the projection on the eigenvectors 340 to 450 and 1000 at $\theta = 19\pi/40$

As an alternative, that avoids the large value of the biggest eigenvalue, we may shift both the typical signals and the real data to zero mean signals. In this case there is no eigenvalue much larger than all others. The left panel of figure 7 displays a 3D plot of the tomogram for the 1000 coefficients obtained with zero mean signals. We have also applied a denoising procedure, removing the small coefficients. The right panel in figure 7 shows the projection on the eigenvectors 340 to 450 at $\theta = 19\pi/40$. One sees that the pressure drop produced by the dust devil is completely separated from any other components in the signal.

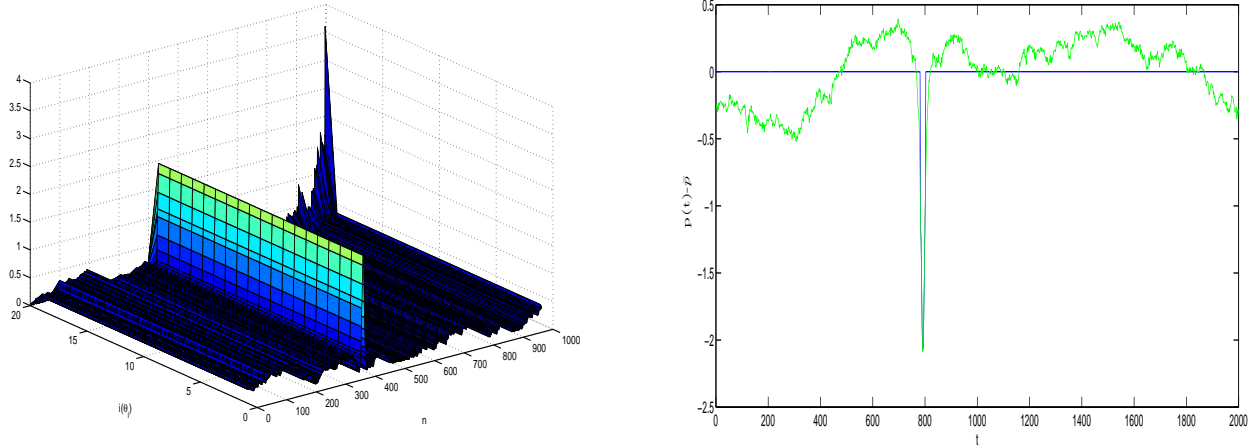


Figure 7: Tomogram for 0 mean typical signals and the projection on the eigenvectors 340 to 450 at $\theta = 19\pi/40$

4 Conclusions

Tomograms provide a two-variable characterization of signals which, due to its rigorous probabilistic interpretation, is robust and free of artifacts and ambiguities. For each particular signal that one wants to analyze, the choice of the appropriate tomogram depends not only on the signal but also on the features that we might want to identify or emphasize.

We have developed a new family of data-driven tomograms that are combination of time and an operator obtained from a set of typical signals specially tuned to represent the features that one wants to extract. These adapted tomograms provide, for noisy signals, filtering and separation of components and features that might not be well represented by the combination of standard operators.

Acknowledgments

This work is partially supported by Spanish MICINN BFU2009-08473 and MEIGA METNET PRECURSOR (AYA2011-29967-C05-02) funded by the Spanish Ministerio de Economía y Competitividad. We would also like to thank Germán Martínez for providing the Phoenix Mars Lander data.

References

- [1] A. D. Poularikas (ed.); *The Transforms and Applications Handbook*, CRC Press & IEEE Press, Boca Raton, Florida (1996).
- [2] K.-B. Wolf; *Integral Transforms in Science and Engineering*, Plenum Press, New York (1979).
- [3] J. B. J. Fourier; *Théorie Analytique de la Chaleur*, in: G. Darbous (ed.), *Oeuvres de Fourier*, Gauthiers-Villars, Paris (1888), Tome premier.
- [4] J. M. Combes, A. Grossmann, and Ph. Tchamitchian (eds.); *Wavelets*, Springer, Berlin (1990), 2nd edition.
- [5] I. Daubechies; *The wavelet transform: time–frequency localization and signal analysis*, IEEE Trans. Inform. Theory, **36**, No. 5 (1990) 961–1005.
- [6] C. K. Chui (ed.); *Wavelets: A Tutorial. Theory and Applications*, Academic, Boston (1992), Vol. 2.
- [7] E. Wigner; *On the quantum correction for thermodynamic equilibrium*, Phys. Rev., 40 (1932) 749–759.
- [8] J. Ville; *Théorie et applications de la notion de signal analytique*, Cables et Transmission, 2 A (1948) 61–74.
- [9] L. Cohen; *Generalized phase-space distribution functions*, J. Math. Phys. 7 (1966) 781–806.
- [10] L. Cohen; *Time–frequency distributions. A review*, Proc. IEEE 77 (1989) 941–981.
- [11] S. Qian and D. Chen; *Joint time–frequency analysis*, Prentice-Hall, Englewood Cliffs, N. J. (1995).
- [12] K. Husimi; *Some formal properties of the density matrix*, Proc. Phys. Mat. Soc. Jpn, 22 (1940) 264–314.
- [13] Y. Kano; *A new phase-space distribution function in the statistical theory of the electromagnetic field*, J. Math. Phys. 6 (1965) 1913–1915.
- [14] V. I. Man’ko and R. Vilela Mendes; *Noncommutative time–frequency tomography*, Phys. Lett. A, 263 (1999) 53–59.

- [15] M. A. Man'ko, V. I. Man'ko and R. Vilela Mendes; *Tomograms and other transforms: A unified view*, J. Phys. A: Math. and Gen.34 (2001) 8321-8332.
- [16] F. Briolle, V. I. Man'ko, B. Ricaud and R. Vilela Mendes; *Non-commutative tomography: A tool for data analysis and signal processing*, Journal of Russian Laser Research 33 (2012) 103-121.
- [17] S. R. Deans; *The Radon Transform and Some of Its Applications*, John Wiley & Sons, New York 1983.
- [18] J. C. Woods and D. T. Barry; *Linear signal synthesis using the Radon-Wigner transform*, IEEE Trans. Signal Process. 42 (1994) 2105–2111.
- [19] S. Granieri, W. D. Furlan, G. Saavedra, and P. Andrés; *Radon-Wigner display: a compact optical implementation with a single varifocal lens*, Appl. Opt. 36 (1997) 8363–8369.
- [20] J. Bertrand and P. Bertrand; *A class of affine Wigner functions with extended covariance properties*, J. Math. Phys., 33 (1992) 2515–2527.
- [21] P. Goncalvés and R. G. Baraniuk; *A pseudo-Bertrand distribution for time-scale analysis*, IEEE Signal Process. Lett. 3 (1996) 82–84.
- [22] F. Briolle, R. Lima, V. I. Man'ko and R. Vilela Mendes; *A tomographic analysis of reflectometry data I: Component factorization*, Meas. Sci. Technol. 20 (2009) 105501.
- [23] F. Briolle, R. Lima and R. Vilela Mendes; *A tomographic analysis of reflectometry data II: The phase derivative*, Meas. Sci. Technol. 20 (2009) 105502.
- [24] B. Ricaud, F. Briolle and F. Clairet; *Analysis and separation of time-frequency components in signals with chaotic behavior*, arXiv:1003.0734.
- [25] C. Aguirre, P. Pascual, D. Campos and E.Serrano; *Single neuron transient activity detection by means of tomography*, BMC Neuroscience 2011, 12(Suppl 1):P297

- [26] J. A. Dente, R. Vilela Mendes, A. Lambert and R. Lima; *The bi-orthogonal decomposition in image processing: Signal analysis and texture segmentation*, Signal Processing: Image Communication 8 (1996) 131–148.
- [27] Smith, P. H., et al.; *Introduction to special section on the Phoenix Mission: Landing Site Characterization Experiments, Mission Overviews, and Expected Science*, J. Geophys. Res., 113, E00A18 (2008).
- [28] E. de Lucas, M. J. Miguel, D. Mozos, and L. Vázquez; *Martian dust devils detector over FPGA*, Geosci. Instrum. Method. Data Syst., 1, 23–31, (2012)